Jiangyong Liu[1,2]
Dan Wang[1,2]
Min Wang[2]
Dejia Kong[3]
Yi Zhang[1]
Jian-Feng Chen[1]
Liming Dai[2]

[1]State Key Laboratory of Organic-Inorganic Composites, Research Center of the Ministry of Education for High Gravity Engineering and Technology, Department of Chemical Engineering, Beijing University of Chemical Technology, Beijing, China.

[2]Center of Advanced Science and Engineering for Carbon (Case4Carbon), Department of Macromolecular Science and Engineering, Case School of Engineering, Case Western Reserve University, Cleveland, OH, USA.

[3]Department of Chemical Engineering, Columbia University, New York, NY, USA.

Supporting Information available online

Uniform Two-Dimensional Co_3O_4 Porous Sheets: Facile Synthesis and Enhanced Photocatalytic Performance

The preparation of high-quality two-dimensional materials with highly interesting properties and applications, such as graphene and graphene analogues, is a rapidly expanding research area. Herein, two-dimensional porous Co_3O_4 sheets with high uniformity were synthesized via a facile hydrothermal route. Various characterizations were performed to investigate this sheet-like structure. Owing to the desired promotion effects and multiple functionalities derived from this unique structure, the porous Co_3O_4 sheets present an enhanced photocatalytic performance in comparison with the bulk Co_3O_4 powder.

Keywords: Co_3O_4, Dye degradation, Photocatalysis, Porous sheets, Two-dimensional structure

Received: September 9, 2015; *revised:* December 20, 2015; *accepted:* January 12, 2016

DOI: 10.1002/ceat.201500542

1 Introduction

Earth-abundant, scalable and nonprecious cobalt oxides, with exceptional physical and chemical properties, have aroused much attention in recent years for their great potential applications [1–4]. Tricobalt tetraoxide (Co_3O_4), the most stable phase in the Co–O system, is a mixed-valence compound [$Co^{II}Co^{III}_2O_4$] with a spinel crystal structure based on a cubic close packing array of oxide ions, in which Co(II) ions occupy the tetrahedral 8a sites and Co(III) ions occupy the octahedral 16d sites [5, 6]. Co_3O_4 has exhibited outstanding performances in view of its applications in the field of lithium batteries [7], supercapacitors [8], gas sensors [9], heterogeneous catalysis [10], etc.

It is well known that the ultimate performance and application of nanomaterials are significantly dependent on their morphologies and microstructures [11]. Compounds with the same chemical compositions but different morphologies and microstructures can give rise to substantial differences in performance. Therefore, morphology control of materials has stimulated great research interests and has been widely investigated by the academic community [12–14]. Many reports are available on the synthesis of Co_3O_4 materials, and a wide variety of morphologies have been explored, such as zero-dimensional (0D) structures (e.g., nanocubes [15] and nanooctahedras [16]), one-dimensional (1D) structures (e.g., nanowires [17] and nanorods [18]), two-dimensional (2D) structures (e.g., nanoplates [19] and nanosheets [20]) and three-dimensional (3D) structures (e.g., nanoflowers [21] and nanonets [22]).

Since the advent of graphene [23], the high-quality 2D nanostructures with exciting properties and applications have

Correspondence: Prof. Jian-Feng Chen (chenjf@mail.buct.edu.cn), State Key Laboratory of Organic-Inorganic Composites, Research Center of the Ministry of Education for High Gravity Engineering and Technology, Department of Chemical Engineering, Beijing University of Chemical Technology, Beijing 100029, China; Prof. Liming Dai (liming.dai@case.edu), Center of Advanced Science and Engineering for Carbon (Case4Carbon), Department of Macromolecular Science and Engineering, Case School of Engineering, Case Western Reserve University, Cleveland 44106, OH, USA.

received continuous interest and are highly desirable for achieving exceptional catalytic, photovoltaic, and electrochemical performances, owing to their large surface-to-volume ratio and confined thickness [24–30]. Other 2D crystals in this rapidly expanding research area include graphene analogues such as boron nitride (BN) [31], transition metal dichalcogenides such as MoS_2 and WS_2 [32], colloidal nanoplatelets such as CdSe and CdS [33], and transition metal oxide nanosheets such as Co_3O_4 and WO_3 [34].

The increasing world energy demand and the growing concerns about environmental issues have continuously motivated extensive research efforts on the heterogeneous photocatalytic technologies [35–37]. As a versatile and important magnetic p-type semiconductor [38, 39], Co_3O_4 has recently been considered as an emerging photocatalytic material and is attracting more and more attention for its excellent photocatalytic performance, great growing potential, and bright prospect in the related fields, such as environmental remediation [40–42] and water splitting [43]. Co_3O_4 with various morphologies, such as its hierarchical 3D porous/urchin nanostructure [40], hierarchical triangular prism structure [41], and bimodal mesoporous structure [42], have been employed for the photocatalytic degradation of pollutants. In this study, it is demonstrated that 2D porous Co_3O_4 sheets with high uniformity, fabricated by a facile and fast hydrothermal method, can serve as an efficient photocatalyst in the degradation of methylene blue (MB), which is a representative of ubiquitous organic pollutants in industrial wastewater.

2 Experimental

The porous Co_3O_4 sheets were prepared by a facile hydrothermal method. In a typical experiment, 0.58 g $Co(NO_3)_2{\cdot}6H_2O$ (≥ 99 %; Acros Organics, USA) was first dissolved in 16 mL deionized water and 4 mL ethanol, followed by the addition of 0.30 g polyvinylpyrrolidone (PVP) K30 (molecular biology reagent grade; MP Biomedicals, USA) under magnetic stirring. Then, 0.36 g of urea (≥ 99 %; Fisher Scientific, USA) was added, with vigorous stirring. Finally, the reaction mixture was sealed in a Teflon-lined stainless-steel autoclave with an internal volume of 45 mL and maintained at 453 K for 4 h. After cooling the autoclave naturally, the precursor was collected by centrifugation and repeated washing with deionized water and ethanol for several times. The obtained precipitate was dried under vacuum at 333 K overnight. The final thermal pyrolysis of the as-synthesized cobalt precursor was performed in flowing air from room temperature to 773 K and maintained at that temperature for 2 h to get the final product. For comparison, the conventional bulk Co_3O_4 powder was prepared as well, by calcining $Co(NO_3)_2{\cdot}6H_2O$ (≥ 99 %; Acros Organics, USA) at 773 K in flowing air. The samples were systematically investigated with various characterizations (see the Supporting Information for experimental details).

Photocatalytic performance of the porous Co_3O_4 sheets was evaluated by the photodegradation of MB (Fisher Scientific, USA). In a typical process, the photocatalyst (10 mg) was suspended in the MB aqueous solution (1×10^{-5} mol L^{-1}, 20 mL) and dispersed under ultrasonic vibration for 10 min. Before irradiation, the suspension was stirred in the dark for 60 min to establish the adsorption–desorption equilibrium between the dye solution and the catalyst. The degradation was performed at ambient temperature under irradiation with 365-nm UV light (Spectroline, model ENF-240C; Spectronics Co., Westbury, NY, USA). It should be noted that no H_2O_2 or air bubbling was added or performed in the reaction process. At given time intervals, the suspension was withdrawn regularly and centrifuged. The supernatant was analyzed with a UV-VIS spectrophotometer (Jasco V-670 EX; Japan) to record MB concentrations at a wavelength of 664 nm. MB degradation was expressed as C/C_0 versus the UV irradiation time, where C is the MB concentration at time t and C_0 is the initial MB concentration.

3 Results and Discussion

3.1 Phase, Texture and Morphologies

As shown in Fig. 1, the characteristic X-ray diffraction (XRD) peaks of the cobalt precursor can be well indexed to the cobalt hydroxide carbonate [$Co_2(OH)_2CO_3$] phase (JCPDS 1-1024) [44]. After heat treatment, the obtained sample can be distinguished as Co_3O_4, with all the diffraction peaks well indexed to the Co_3O_4 spinel phase (JCPDS 42-1467) [45], and no other crystalline phases are observed, thereby confirming the high purity of the material. Moreover, the sharp diffraction peaks of both samples suggest a high crystallinity of the synthesized materials.

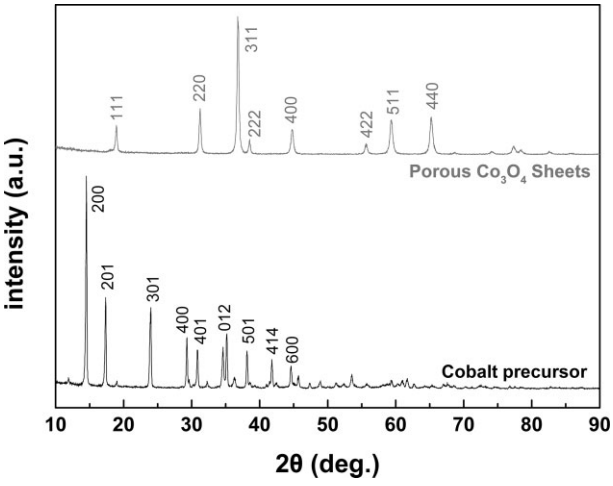

Figure 1. XRD patterns of the cobalt precursor and the porous Co_3O_4 sheets.

Fig. 2 presents representative scanning electron microscopy (SEM) images of the cobalt precursor (Fig. 2 a) and the porous Co_3O_4 sheets (Fig. 2 b–d). It can be clearly observed that the cobalt precursor $Co_2(OH)_2CO_3$ is composed of uniform sheet-like structures, and the surface of the sheets shows a very smooth texture. After thermal pyrolysis, porous Co_3O_4 sheets with a rough appearance are successfully obtained, with the original sheet structure well maintained and numerous pores

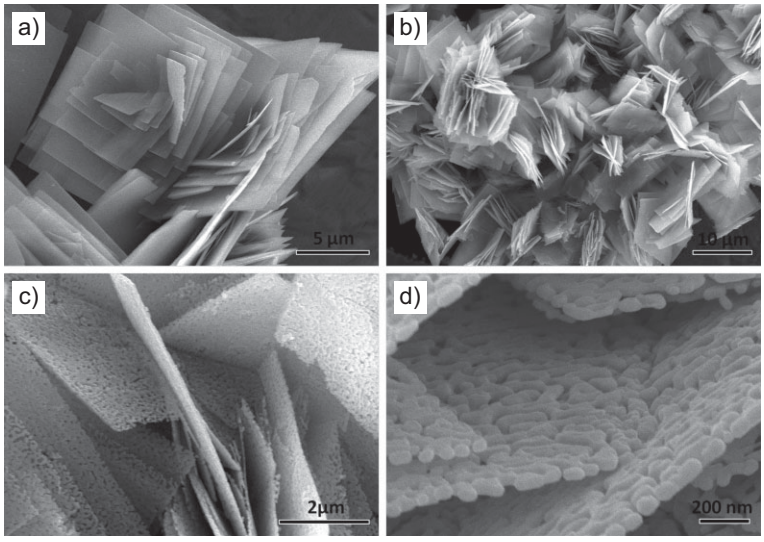

Figure 2. (a) SEM images of the cobalt precursor. (b–d) SEM images of the porous Co_3O_4 sheets at various magnifications.

generated. For the bulk Co_3O_4 powder, however, only significantly aggregated and irregular-shaped particles can be observed (see Supporting Information Fig. S1). Energy-dispersive spectroscopy (EDS) analysis (Fig. 3 a) clearly manifests that the porous Co_3O_4 sheets are composed of Co and O, with a molar ratio of 2.98:1, very close to the stoichiometric composition of the Co_3O_4 phase. The signal of C comes from the adhesive carbon tape. The EDS elemental mapping (Fig. 3 b) performed on an individual Co_3O_4 sheet reveals the homogeneous element distribution of Co and O in the porous Co_3O_4 sheets.

The transmission electron microscopy (TEM) images displayed in Fig. 4 a provide a direct observation of the morphology and distribution of the Co_3O_4 particles in the porous Co_3O_4 sheets. It can be observed that the porous sheets are composed of highly dispersed Co_3O_4 particles and numerous pores. Other important information about the chemical composition of the products is further provided by the X-ray photoelectron spectroscopy (XPS) measurements, as shown in Fig. 4 c. The Co 2p XPS spectrum shows two major peaks with binding energies at 781.2 and 796.3 eV (with spin-orbital splitting of 15.1 eV), corresponding to Co $2p_{3/2}$ and Co $2p_{1/2}$, respectively, characteristic of the pure Co_3O_4 phase [46, 47]. The N_2 adsorption–desorption isotherm of the porous Co_3O_4 sheets (Fig. 4 d) can be categorized as type IV, with a hysteresis loop [48]. And the average pore diameter is 16.5 nm, according to the corresponding pore size distribution (PSD) calculated from the desorption branch by the Barrett-Joyner-Halenda (BJH) model, indicating the presence of mesoscale pores. The Brunauer-Emmett-Teller (BET) surface area of the porous Co_3O_4 sheets is measured to be 23.6 m^2g^{-1}, which is much higher than that of the bulk Co_3O_4 powder (6.2 m^2g^{-1}, a normal value of Co_3O_4 prepared by simple calcinations) [49].

Based on the characterization results and the above discussion, the formation mechanism of the porous Co_3O_4 sheets with high uniformity can be reasonably inferred. Both the hydrothermal process and the following calcination process are crucial for the final obtainment of the uniform porous Co_3O_4 sheets with the textural characteristics of intracrystalline mesopores. When heated in aqueous solution, the slow hydrolysis of urea at elevated temperature can gradually produce alkaline media and release both hydroxyl and carbonate ions, which can initiate the precipitation of Co^{2+} in the solution to form the precursor with progressing reaction time. This homogeneous and controllable precipitation process gives rise to slow crystal growth of the materials and is beneficial for the shape control of the crystals [50]. In addition, the polymer-directing agent PVP has an important effect on the morphology of the materials and can act as a multifunctional additive during the hydrothermal process. When added, the PVP molecules can selectively adsorb onto the crystal faces, induce the growth and crystallization of the intermediate crystal nucleus, and lead the subsequent assembly of the final sheet-like structure. It is generally considered that preferential adsorption of molecules and ions in solution to different crystal faces results in various morphologies by controlling the growth rates along different crystal directions [51]. After heat treatment, the final porous Co_3O_4 sheets are obtained, which can be attributed to the successive release of H_2O and CO_2 gas from

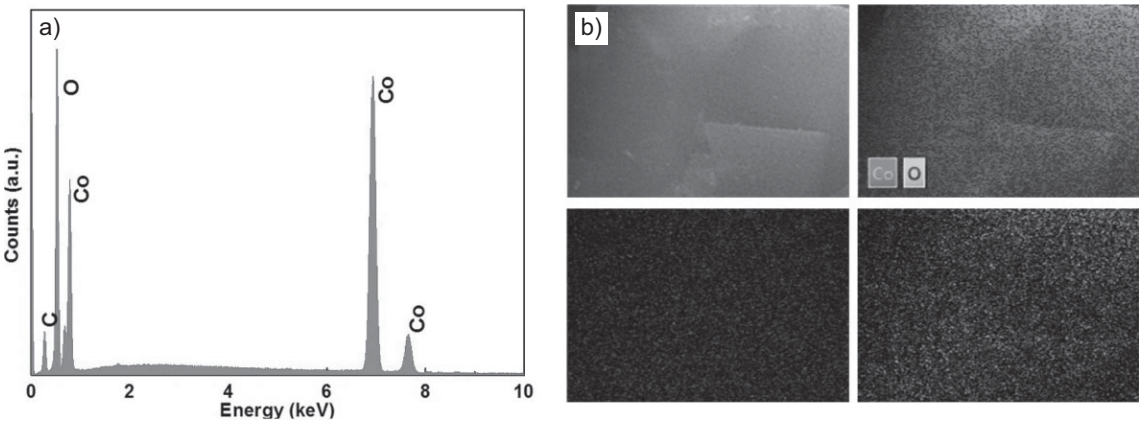

Figure 3. (a) EDS analysis and (b) elemental mapping of an individual Co_3O_4 porous sheet.

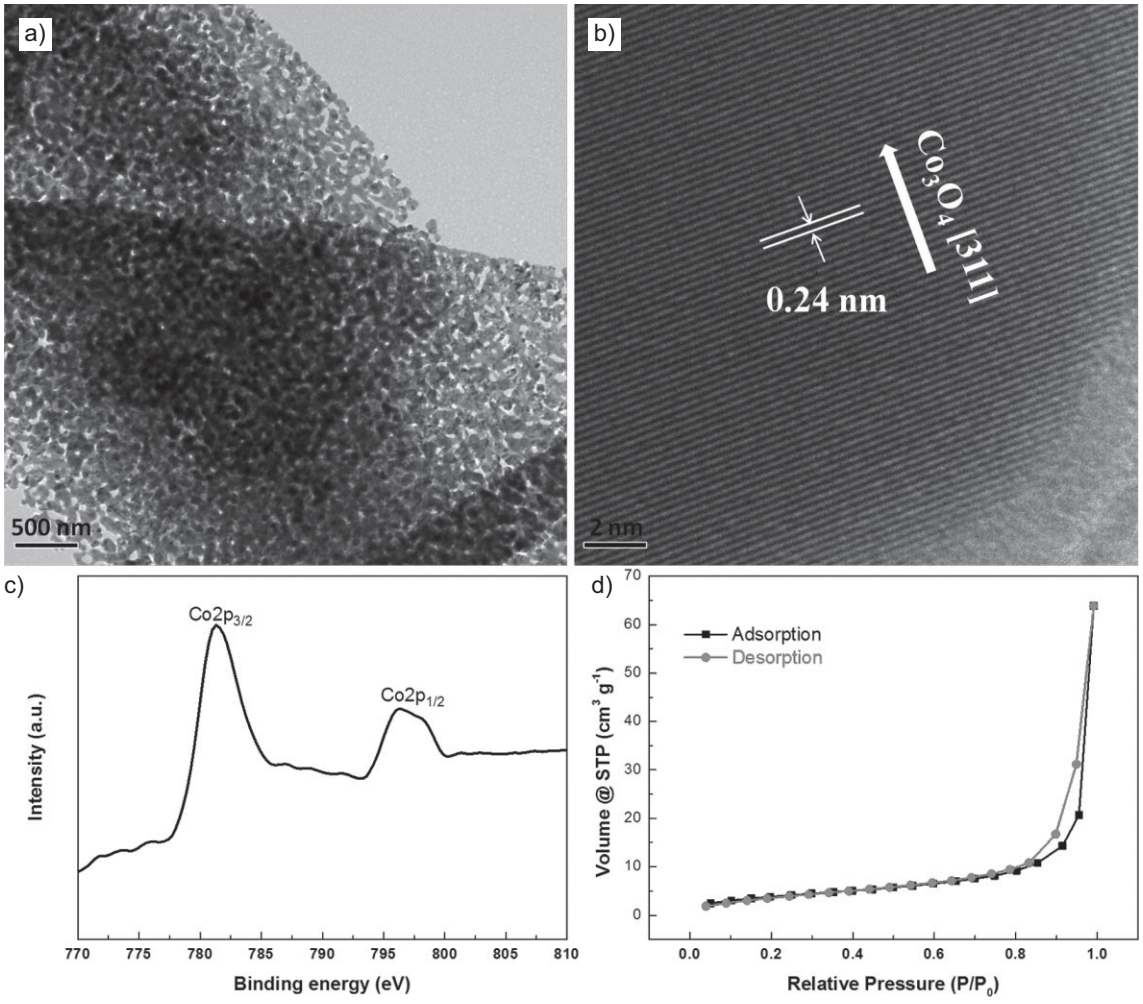

Figure 4. (a) TEM images of the porous Co_3O_4 sheets, (b) high-resolution TEM image of the Co_3O_4 phase, (c) XPS pattern, and (d) nitrogen adsorption-desorption isotherm of the porous Co_3O_4 sheets.

the cobalt precursor during the thermal decomposition process.

3.2 Optical Properties

The optical adsorption profiles of the porous Co_3O_4 sheets and bulk Co_3O_4 powder in the UV-VIS region are shown in the insets of Fig. 5 a and 5 b, respectively. The corresponding band gap energy can be determined by the equation:

$$(\alpha h\nu)^n = B(h\nu - E_g) \quad (1)$$

where $h\nu$ is the photo energy, E_g is the band gap, B is a constant related to the material, n is a value that depends on the nature of the transition (for a direct transition, n equals 2), and α is the absorption coefficient [52]. The $(\alpha h\nu)^n$ versus $h\nu$ (Tauc plot) extrapolated to $\alpha = 0$ gives the absorption band gap energies, as exhibited in Fig. 5a, b for the porous Co_3O_4 sheets and bulk Co_3O_4 powder, respectively. The Tauc plot profiles of both samples give two band gap energies. The higher band gap is assigned to the $O^{2-} \rightarrow Co^{2+}$ charge transfer process (basic optical band gap energy or valence to conduction band excitation), while the lower band gap is ascribed to the $O^{2-} \rightarrow Co^{3+}$ charge transfer process (with Co^{3+} located below the conduction band). The presence of Co^{3+} centers in Co_3O_4 produces a subband located inside the energy gap [18].

The band edge positions of the photocatalysts can be calculated according to the Mulliken electronegativity. The conduction band (CB) and valence band (VB) potentials of the samples can be calculated by the following equations:

$$E_{VB} = X - E_e + \frac{1}{2}E_g \quad (2)$$

$$E_{CB} = E_{VB} - E_g \quad (3)$$

where E_e is the energy of free electrons on the hydrogen scale (~4.5 eV), E_g is the band gap energy of the photocatalyst, and X ($X = (X_1X_2X_3\ldots X_n)^{1/n}$, ~5.903 eV for Co_3O_4) is the absolute electronegativity of the semiconductor and is defined as the geometric mean of the absolute electronegativity of the constit-

uent atom. On the basis of the above equations, the top of the VB and the bottom of the CB of the porous Co_3O_4 sheets are calculated to be 2.783 and 0.023 eV, respectively. Accordingly, the VB and CB of the bulk Co_3O_4 powder are estimated to be 2.473 and 0.333 eV, respectively [53]. In a recently published work [2], the authors show that the high photocatalytic activity of CoO nanoparticles arises from a significant shift in the position of the band edge of the material, while CoO micropowders with improper band edges are inactive. In our study, we also observe that the band edge of the porous Co_3O_4 sheets has shifted compared with the bulk sample, which is similar to the previous result and shows the importance of the morphology effect on the band edge. Compared with the bulk Co_3O_4 powder, the porous Co_3O_4 sheet has a lower VB position, indicating a stronger photooxidative capability which enables the photogenerated holes to have a large thermodynamic driving force to directly engage in the degradation process [54].

3.3 Photocatalytic Test

MB is widely used in the textile and dyestuff manufacturing industries and can provoke serious environmental problems in the neighboring receptor water bodies [55]. To evaluate the photocatalytic performance of the porous Co_3O_4 sheets, the degradation of MB under UV light irradiation is employed as a model example. The conventional bulk Co_3O_4 powder was tested as well under the same conditions for a better comparison. As shown in Fig. 6 b, it can be observed that, without photocatalyst (MB photolysis), only a small amount of MB was degraded. However, when the catalysts were applied, the degradation of MB was apparently accelerated. It is obvious that the porous Co_3O_4 sheets exhibited a higher photocatalytic activity than the bulk Co_3O_4 powder. Within the reaction duration, about 90.0 % of the MB was degraded, as evidenced by the rapid decrease of the maximum absorption peak at 664 nm and the color changes of the MB solution (Fig. 6 a). However, the degradation efficiency of the bulk Co_3O_4 powder is only about 42.7 %, which is significantly lower than that of the porous Co_3O_4 sheets.

It has been generally considered that the photocatalytic degradation of MB solutions agrees with pseudo-first-order kinetics, and can be illustrated by Eq. (4):

$$\ln(C_{ads}/C) = kt \quad (4)$$

where C_{ads} and C are the concentrations of MB after dark adsorption and at time t, respectively [56, 57]. Fig. 6 c shows the linear relationship of $\ln(C_{ads}/C)$ versus the irradiation time. As a result, a plot of $\ln(C_{ads}/C)$ versus t can yield the apparent rate constant for the degradation of MB from the slope of the curve fitting line. The apparent rate constants were calculated to be 0.0069 and 0.0016 min^{-1} for the porous Co_3O_4 sheets and bulk Co_3O_4 powder, respectively. All these results suggest that the uniform porous Co_3O_4 sheets are efficient in the degradation of MB and have application potential in wastewater treatment. Compared with the bulk Co_3O_4 powder, the porous Co_3O_4 sheets exhibit superior photocatalytic activity.

It is generally accepted that the adsorption and desorption of molecules on the catalyst surface has a significant impact on the ultimate catalytic performance. The catalyst that absorbs more organic pollutants tends to have better photocatalytic activity. Compared with the bulk Co_3O_4 powder, the porous Co_3O_4 sheets should adsorb much more MB molecules during the reaction process due to their higher BET surface area, as mentioned above. The high adsorption capability of the porous Co_3O_4 sheets can be inferred from the large amount of MB removed under dark conditions before exposure to UV irradiation. The porous Co_3O_4 sheets possess more unsaturated surface coordination sites and can absorb more dye pollutant. When Co_3O_4 is illuminated by the UV light, reactive oxygen species (ROS), such as hydroxyl ($^{\bullet}OH$), superoxide ($^{\bullet}O_2^-$), and hydrogen peroxide ($HO_2^{\bullet}$), can be generated, which degrade the organic compounds adsorbed on the catalyst surface [58, 59]. Moreover, the porous sheet-like structure with strong photooxidative capability can facilitate the fast diffusion of dye

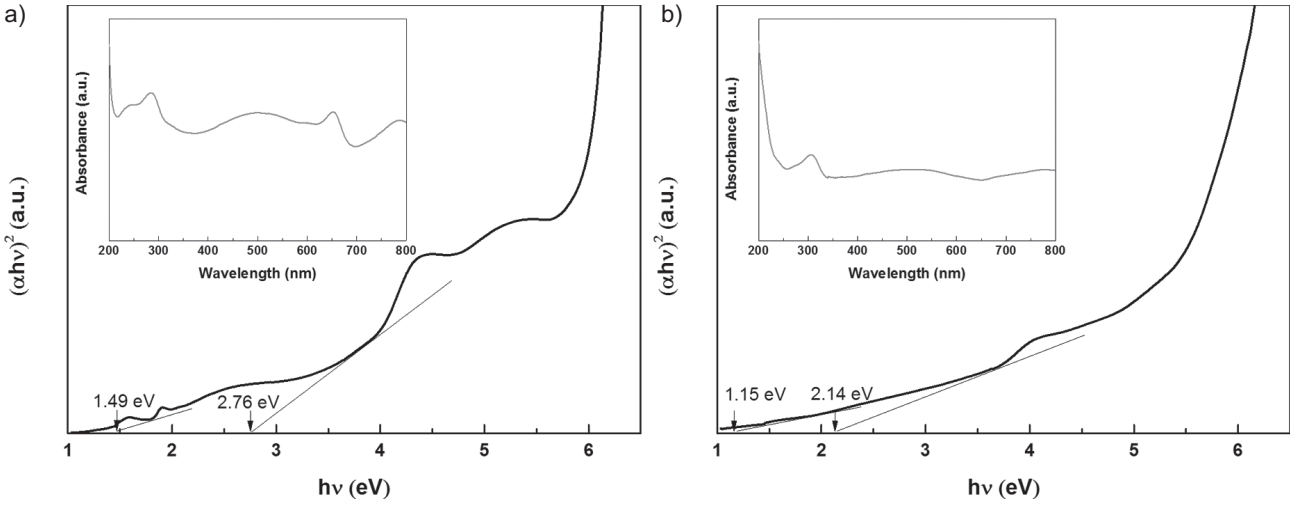

Figure 5. Optical band gap energy of (a) the porous Co_3O_4 sheets and (b) the bulk Co_3O_4 powder obtained by the extrapolation of $\alpha = 0$. Insets show the corresponding UV-VIS absorption spectra of the samples.

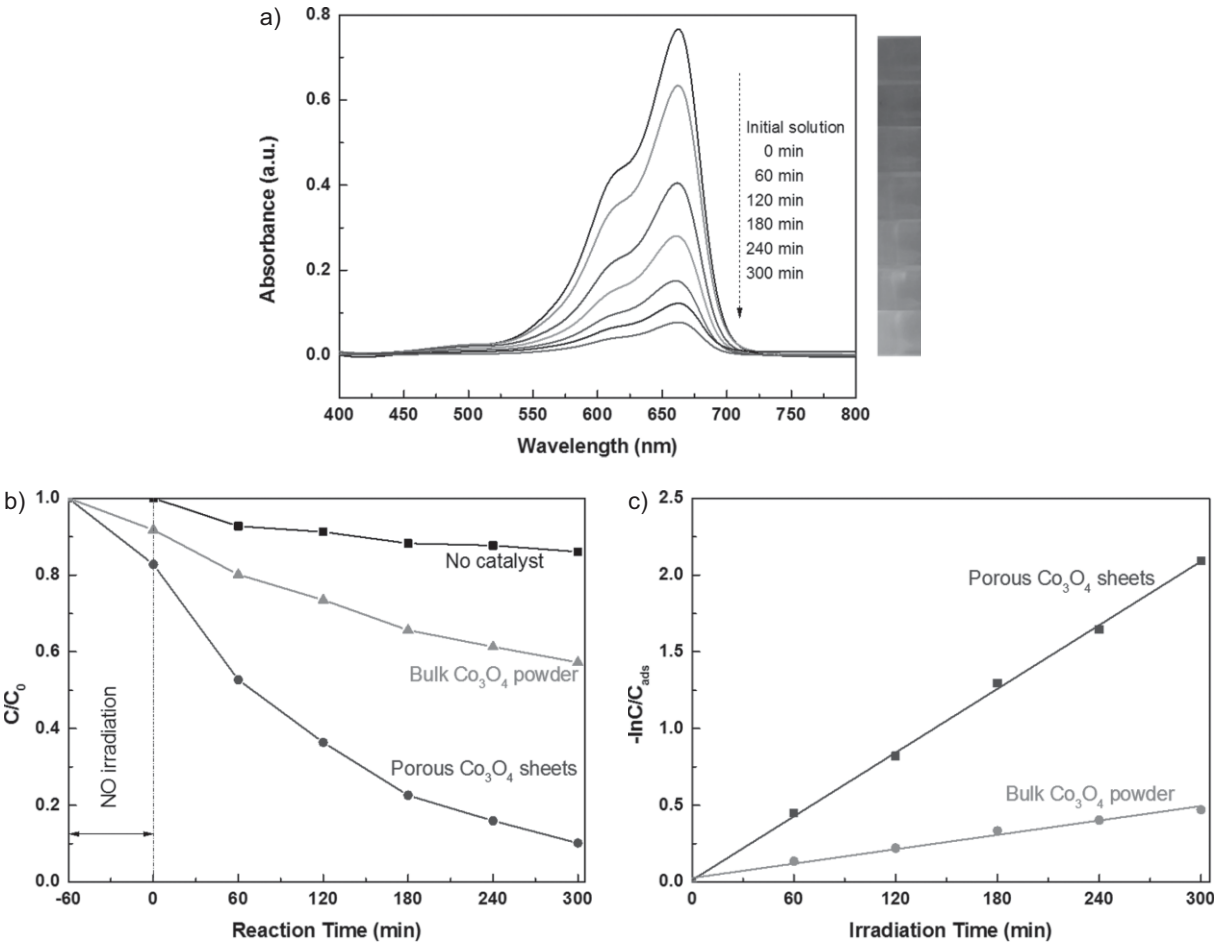

Figure 6. (a) UV-VIS spectroscopic changes of MB over the porous Co_3O_4 sheets under UV irradiation. (b) Degradation rate of MB under UV irradiation in the presence and absence of catalysts. (c) The first-order kinetics of MB degradation under UV irradiation over the porous Co_3O_4 sheets and the bulk Co_3O_4 powder.

molecules, relieving the mass transfer restrictions, which is beneficial to an enhancement of the photocatalytic activity. Also, the 2D Co_3O_4 sheets can act as an excellent transport platform to promote charge transportation, and therefore the recombination process of the electron-hole pairs is hindered, providing more photogenerated charge carriers for the associated photocatalytic reactions [60, 61]. Photoluminescence spectroscopy measurements were performed to support this explanation. It is generally considered that higher fluorescence intensity indicates more recombination of the electron-hole pairs and thus weaker photocatalytic activity [62]. As displayed in Supporting Information Fig. S2, both the porous Co_3O_4 sheets and the bulk Co_3O_4 powder show weak photoluminescence peaking at 520 nm under excitation by 325-nm UV light [63, 64]. However, the emission intensity of the porous Co_3O_4 sheets was much lower than that of the bulk Co_3O_4 powder, indicating the lower recombination rate of the photogenerated charge carriers. Furthermore, the porous stacked sheets can result in multiple reflections [65, 66] among the gaps of the stacking Co_3O_4 sheets, and thus can absorb more incident UV light, which can be another reason for the high phtotocatalytic activity associated with the structure. In short, all these factors can be reasonably employed to explain the remarkably better photocatalytic performance of the porous Co_3O_4 sheets, as compared with the bulk Co_3O_4 powder. And the above-proposed descriptions provide some useful information on the optimal design of an efficient photocatalyst for the degradation process.

The Fourier-transform infrared (FT-IR) spectra of the spent porous Co_3O_4 sheets indicate that the peaks are similar to those of the original material, and none of peaks of the dye molecules can be distinguished, as shown in Supporting Information Fig. S3. This observation suggests that MB is indeed degraded by the photocatalytic effect after the reaction, and not by the adsorption on the catalyst surface. The durability of the porous Co_3O_4 sheets for the MB degradation was also investigated. As shown in Fig. 7, no apparent decrease in the photocatalytic activity can be observed during their repeated use for three times. These results demonstrate that the porous Co_3O_4 sheets as an efficient photocatalyst are stable under the conditions of the experimental reaction process employed here.

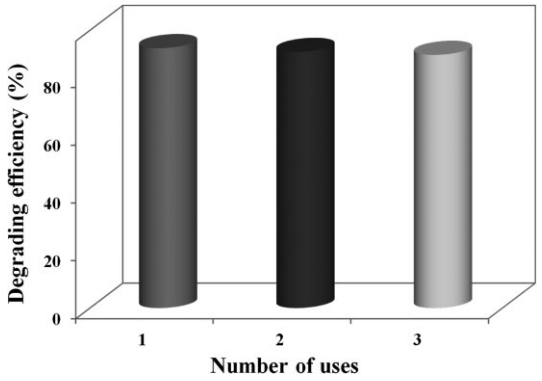

Figure 7. Evaluation of the durability of the porous Co_3O_4 sheets for repeated degradation of MB.

4 Conclusions

In conclusion, uniform 2D Co_3O_4 porous sheets were successfully developed in this study. The produced Co_3O_4 porous sheets were characterized by XRD, SEM, TEM, EDS, etc. The application of this kind of porous Co_3O_4 sheets in photocatalytic dye degradation led to multiple functionalities that promoted the photocatalytic activity and exhibited high reaction stability. The characterization results and theoretical analysis suggest that the remarkable catalytic performance of the porous Co_3O_4 sheets as an efficient photocatalyst can be rationally attributed to the good adsorption ability, the high transportation efficiency, and the optimized reaction environment. In addition to the facile preparation process and excellent reaction performance, preliminary findings suggest that the uniform porous Co_3O_4 sheets presented here are a promising material for water purification and other chemical processes. More studies on the materials will be helpful to understand the mechanism of the nanostructure formation and to optimize the structure of the materials, which should be good topics for future studies.

Acknowledgment

This work was financially supported by the "111" project of China (No. B14004), the Foundation of State Key Laboratory of Organic-Inorganic Composites, the Fundamental Research Funds for the Central Universities, and the National Natural Science Foundation of China.

The authors have declared no conflict of interest.

Abbreviations

BET	Brunauer-Emmett-Teller
CB	conduction band
EDS	energy-dispersive spectroscopy
MB	methylene blue
PVP	polyvinylpyrrolidone
SEM	scanning electron microscopy
TEM	transmission electron microscopy
VB	valence band
XPS	X-ray photoelectron spectroscopy
XRD	X-ray diffraction

References

[1] X. Xie, Y. Li, Z. Q. Liu, M. Haruta, W. Shen, *Nature* **2009**, *458*, 746–749. DOI: 10.1038/nature07877

[2] L. Liao, Q. Zhang, Z. Su, Z. Zhao, Y. Wang, Y. Li, X. Lu, D. Wei, G. Feng, Q. Yu, X. Cai, J. Zhao, Z. Ren, H. Fang, F. Robles-Hernandez, S. Baldelli, J. Bao, *Nat. Nanotechnol.* **2014**, *9*, 69–73. DOI: 10.1038/nnano.2013.272

[3] H. Hu, B. Guan, B. Xia, X. W. Lou, *J. Am. Chem. Soc.* **2015**, *137 (16)*, 5590–5595. DOI: 10.1021/jacs.5b02465

[4] J. Y. Liu, J. F. Chen, Y. Zhang, *RSC Adv.* **2015**, *5 (77)*, 62931–62935. DOI: 10.1039/C5RA10005D

[5] D. Barreca, C. Massignan, S. Daolio, M. Fabrizio, C. Piccirillo, L. Armelao, E. Tondello, *Chem. Mater.* **2001**, *13 (2)*, 588–593. DOI: 10.1021/cm001041x

[6] X. Wang, X. Chen, L. Gao, H. Zheng, Z. Zhang, Y. Qian, *J. Phys. Chem. B* **2004**, *108 (42)*, 16401–16404. DOI: 10.1021/jp048016p

[7] J. Wang, N. Yang, H. Tang, Z. Dong, Q. Jin, M. Yang, D. Kisailus, H. Zhao, Z. Tang, D. Wang, *Angew. Chem. Int. Ed.* **2013**, *52 (25)*, 6417–6420. DOI: 10.1002/anie.201301622

[8] H. Du, L. Jiao, Q. Wang, J. Yang, L. Guo, Y. Si, Y. Wang, H. Yuan, *Nano Res.* **2013**, *6 (2)*, 87–98. DOI: 10.1007/s12274-012-0283-5

[9] Y. Lü, W. Zhan, Y. He, Y. Wang, X. Kong, Q. Kuang, Z. Xie, L. Zheng, *ACS Appl. Mater. Interfaces* **2014**, *6 (6)*, 4186–4195. DOI: 10.1021/am405858v

[10] J. Xu, P. Gao, T. S. Zhao, *Energy Environ. Sci.* **2012**, *5 (1)*, 5333–5339. DOI: 10.1039/C1EE01431E

[11] D. Wang, J. Qian, F. Cai, S. He, S. Han, Y. Mu, *Nanotechnology* **2012**, *23 (24)*, 245701. DOI: 10.1088/0957-4484/23/24/245701

[12] M. Pudukudy, Z. Yaakob, *Chem. Papers* **2014**, *68 (8)*, 1087–1096. DOI: 10.2478/s11696-014-0561-7

[13] S. Verma, D. Verma, S. L. Jain, *Tetrahedron Lett.* **2014**, *55 (15)*, 2406–2409. DOI: 10.1016/j.tetlet.2014.02.120

[14] S. Verma, R. B. Nasir Baig, C. Han, M. N. Nadagouda, R. S. Varma, *Chem. Commun.* **2015**, *51 (85)*, 15554–15557. DOI: 10.1039/C5CC05895C

[15] X. Liu, Q. Long, C. Jiang, B. Zhan, C. Li, S. Liu, Q. Zhao, W. Huang, X. Dong, *Nanoscale* **2013**, *5 (14)*, 6525–6529. DOI: 10.1039/C3NR00495C

[16] X. Wang, L. Yu, X. L. Wu, F. Yuan, Y. G. Guo, Y. Ma, J. Yao, *J. Phys. Chem. C* **2009**, *113 (35)*, 15553–15558. DOI: 10.1021/jp904652m

[17] Y. Li, B. Tan, Y. Wu, *J. Am. Chem. Soc.* **2006**, *128 (44)*, 14258–14259. DOI: 10.1021/ja065308q

[18] G. Wang, X. Shen, J. Horvat, B. Wang, H. Liu, D. Wexler, J. Yao, *J. Phys. Chem. C* **2009**, *113 (11)*, 4357–4361. DOI: 10.1021/jp8106149

[19] F. Wang, C. Lu, Y. Qin, C. Liang, M. Zhao, S. Yang, Z. Sun, X. Song, *J. Power Sources* **2013**, *235*, 67–73. DOI: 10.1016/j.jpowsour.2013.01.190

[20] X. Wang, H. Guan, S. Chen, H. Li, T. Zhai, D. Tang, Y. Bando, D. Golberg, *Chem. Commun.* **2011**, *47 (45)*, 12280–12282. DOI: 10.1039/C1CC15169J
[21] Y. Zhang, Y. Chen, T. Wang, J. Zhou, Y. Zhao, *Microporous Mesoporous Mater.* **2008**, *114 (1)*, 257–261. DOI: 10.1016/j.micromeso.2008.01.011
[22] Y. Wang, Y. Lei, J. Li, L. Gu, H. Yuan, D. Xiao, *ACS Appl. Mater. Interfaces* **2014**, *6 (9)*, 6739–6747. DOI: 10.1021/am500464n
[23] K. S. Novoselov, A. K. Geim, S. V. Morozov, D. Jiang, Y.Zhang, S. V. Dubonos, I. V. Grigorieva, A. A. Firsov, *Science* **2004**, *306*, 666–669. DOI: 10.1126/science.1102896
[24] R. Jabari-Seresht, M. Jahanshahi, A. Rashidi, A. A. Ghoreyshi, *Chem. Eng. Technol.* **2013**, *36 (9)*, 1550–1558. DOI: 10.1002/ceat.201300002
[25] D. Wang, J. F. Chen, L. Dai, *Part. Part. Syst. Charact.* **2015**, *32 (5)*, 515–523. DOI: 10.1002/ppsc.201400219
[26] D. Verma, S. Verma, A. K. Sinha, S. L. Jain, *ChemPlusChem* **2013**, *78 (8)*, 860–865. DOI: 10.1002/cplu.201300196
[27] H. P. Mungse, S. Verma, N. Kumar, B. Sain, O. P. Khatri, *J. Mater. Chem.* **2012**, *22 (12)*, 5427–5433. DOI: 10.1039/C2JM15644J
[28] D. Wang, L. Zhu, J. F. Chen, L. Dai, *Nanoscale* **2015**, *7 (21)*, 9894–9901. DOI: 10.1039/C5NR01734C
[29] S. Verma, D. Verma, A. K. Sinha, S. L. Jain, *Appl. Catal., A* **2015**, *489*, 17–23. DOI: 10.1016/j.apcata.2014.10.004
[30] S. Verma, H. P. Mungse, N. Kumar, S. Choudhary, S. L. Jain, B. Sain, O. P. Khatri, *Chem. Commun.* **2011**, *47 (47)*, 12673–12675. DOI: 10.1039/C1CC15230K
[31] C. R. Dean, A. F. Young, I. Meric, C. Lee, L. Wang, S. Sorgenfrei, K. Watanabe, T. Taniguchi, P. Kim, K. L. Shepard, J. Hone, *Nat. Nanotechnol.* **2010**, *5 (10)*, 722–726. DOI: 10.1038/nnano.2010.172
[32] Q. H. Wang, K. Kalantar-Zadeh, A. Kis, J. N. Coleman, M. S. Strano, *Nat. Nanotechnol.* **2012**, *7 (11)*, 699–712. DOI: 10.1038/nnano.2012.193
[33] S. Ithurria, M. D. Tessier, B. Mahler, R. P. S. M. Lobo, B. Dubertret, A. L. Efros, *Nat. Mater.* **2011**, *10 (12)*, 936–941. DOI: 10.1038/nmat3145
[34] Z. Sun, T. Liao, Y. Dou, S. M. Hwang, M. S. Park, L. Jiang, J. H. Kim, S. X. Dou, *Nat. Commun.* **2014**, *5*, 3813. DOI: 10.1038/ncomms4813
[35] A. Fujishima, K. Honda, *Nature* **1972**, *238*, 37–38. DOI: 10.1038/238037a0
[36] Y. Su, A. Talla, V. Hessel, T. Noël, *Chem. Eng. Technol.* **2015**, *38 (10)*, 1733–1742. DOI: 10.1002/ceat.201500376
[37] H. Golmojdeh, M. A. Zanjanchi, *Chem. Eng. Technol.* **2013**, *36 (12)*, 2080–2086. DOI: 10.1002/ceat.201300160
[38] B. Varghese, C. H. Teo, Y. Zhu, M. V. Reddy, B. V. Chowdari, A. T. S. Wee, T. B. C. Vincent, C. T. Lim, C. H. Sow, *Adv. Funct. Mater.* **2007**, *17 (12)*, 1932–1939. DOI: 10.1002/adfm.200700038
[39] B. Geng, F. Zhan, C. Fang, N. Yu, *J. Mater. Chem.* **2008**, *18 (41)*, 4977–4984. DOI: 10.1039/B805378B
[40] R. Edla, N. Patel, M. Orlandi, N. Bazzanella, V. Bello, C. Maurizio, G. Mattei, P. Mazzoldi, A. Miotello, *Appl. Catal., B* **2015**, *166*, 475–484. DOI: 10.1016/j.apcatb.2014.11.060
[41] J. Kou, C. Bennett-Stamper, R. S. Varma, *Nanoscale* **2011**, *3*, 4958–4961. DOI: 10.1039/C1NR10826C
[42] M. Pudukudy, Z. Yaakob, B. Narayanan, A. Gopalakrishnan, S. M. Tasirin, *Superlattices Microstruct.* **2013**, *64*, 15–26. DOI: 10.1016/j.spmi.2013.09.012
[43] M. Zhang, M. de Respinis, H. Frei, *Nat. Chem.* **2014**, *6 (4)*, 362–367. DOI: 10.1038/nchem.1874
[44] L. Xie, K. Li, G. Sun, Z. Hu, C. Lv, J. Wang, C. Zhang, *J. Solid State Electrochem.* **2013**, *17*, 55–61. DOI: 10.1007/s10008-012-1856-7
[45] J. Y. Liu, J. F. Chen, Y. Zhang, *Catal. Sci. Technol.* **2013**, *3 (10)*, 2559–2564. DOI: 10.1039/C3CY00458A
[46] M. Long, W. Cai, J. Cai, B. Zhou, X. Chai, Y. Wu, *J. Phys. Chem. B* **2006**, *110 (41)*, 20211–20216. DOI: 10.1021/jp063441z
[47] A. Martínez, C. López, F. Márquez, I. Díaz, *J. Catal.* **2003**, *220 (2)*, 486–499. DOI: 10.1016/S0021-9517(03)00289-6
[48] T. Zhu, J. S. Chen, X. W. Lou, *J. Mater. Chem.* **2010**, *20 (33)*, 7015–7020. DOI: 10.1039/C0JM00867B
[49] S. Xiong, C. Yuan, X. Zhang, B. Xi, Y. Qian, *Chem. Eur. J.* **2009**, *15 (21)*, 5320–5326. DOI: 10.1002/chem.200802671
[50] Z. Zhao, F. Geng, J. Bai, H. M. Cheng, *J. Phys. Chem. C* **2007**, *111 (10)*, 3848–3852. DOI: 10.1021/jp067320a
[51] C. J. Murphy, *Science* **2002**, *298*, 2139–2141. DOI: 10.1126/science.1080007
[52] S. K. Meher, G. R. Rao, *J. Phys. Chem. C* **2011**, *115 (51)*, 25543–25556. DOI: 10.1021/jp209165v
[53] H. Shi, G. Chen, C. Zhang, Z. Zou, *ACS Catal.* **2014**, *4 (10)*, 3637–3643. DOI: 10.1021/cs500848f
[54] S. Chu, Y. Wang, Y. Guo, J. Feng, C. Wang, W. Luo, X. Fan, Z. Zou, *ACS Catal.* **2013**, *3 (5)*, 912–919. DOI: 10.1021/cs4000624
[55] Z. Wu, H. Zhong, X. Yuan, H. Wang, L. Wang, X. Chen, G. Zeng, Y. Wu, *Water Res.* **2014**, *67*, 330–334. DOI: 10.1016/j.watres.2014.09.026
[56] M. J. Height, S. E. Pratsinis, O. Mekasuwandumrong, P. Praserthdam, *Appl. Catal., B* **2006**, *63 (3)*, 305–312. DOI: 10.1016/j.apcatb.2005.10.018
[57] A. Houas, H. Lachheb, M. Ksibi, E. Elaloui, C. Guillard, J. M. Herrmann, *Appl. Catal., B* **2001**, *31 (2)*, 145–147. DOI: 10.1016/S0926-3373(00)00276-9
[58] R. Leary, A. Westwood, *Carbon* **2011**, *49 (3)*, 741–772. DOI: 10.1016/j.carbon.2010.10.010
[59] S. C. Yan, Z. S. Li, Z. G. Zou, *Langmuir* **2009**, *25 (17)*, 10397–10401. DOI: 10.1021/la900923z
[60] J. Liu, H. Bai, Y. Wang, Z. Liu, X. Zhang, D. D. Sun, *Adv. Funct. Mater.* **2010**, *20 (23)*, 4175–4181. DOI: 10.1002/adfm.201001391
[61] J. Du, X. Lai, N. Yang, J. Zhai, D. Kisailus, F. Su, D. Wang, L. Jiang, *ACS Nano* **2011**, *5 (1)*, 590–596. DOI: 10.1021/nn102767d
[62] M. R. Hoffmann, S. T. Martin, W. Choi, D. W. Bahnemann, *Chem. Rev.* **1995**, *95 (1)*, 69–96. DOI: 10.1021/cr00033a004
[63] Z. Dong, Y. Fu, Q. Han, Y. Xu, H. Zhang, *J. Phys. Chem. C* **2007**, *111 (50)*, 18475–18478. DOI: 10.1021/jp075365l
[64] W. Wang, J. Xu, *ACS Appl. Mater. Interfaces* **2015**, *7 (1)*, 415–421. DOI: 10.1021/am506414n
[65] H. Li, Z. Bian, J. Zhu, D. Zhang, G. Li, Y. Huo, H. Li, Y. Lu, *J. Am. Chem. Soc.* **2007**, *129 (27)*, 8406–8407. DOI: 10.1021/ja072191c
[66] Y. Liu, Y. Deng, Z. Sun, J. Wei, G. Zheng, A. M. Asiri, S. B. Khan, M. M. Rahman, D. Zhao, *Small* **2013**, *9 (16)*, 2702–2708. DOI: 10.1002/smll.201300197

